Numerical Heat Transfer, Part A, vol. 18, pp. 129–147, 1990

CALCULATION OF THE TURBULENT BUOYANCY-DRIVEN FLOW IN A RECTANGULAR CAVITY USING AN EFFICIENT SOLVER AND TWO DIFFERENT LOW REYNOLDS NUMBER k–ϵ TURBULENCE MODELS

Lars Davidson
Department of Applied Thermodynamics and Fluid Mechanics, Chalmers University of Technology, S-41296 Göteborg, Sweden

The buoyancy-driven flow in a tall rectangular cavity of 5:1 aspect ratio with a Rayleigh number of 4×10^{10} is calculated using finite volume methods. The CELS solver is extended to be able to handle large density variations. CELS is compared with SIMPLEC, and it is shown to be up to more than 4 times as fast as SIMPLEC. A modified form of a low Reynolds number k–ϵ turbulence model is developed. This model is consistent in its near-wall behavior, and it allows simulation of the decay of grid turbulence. The model developed by Lam and Bremhorst [1] is also tested. Both turbulence models are shown to predict the transitional and relaminarization regions according to experiments.

INTRODUCTION

Turbulent flow, driven or affected by buoyancy, is an important type of flow that arises in many engineering applications. When calculating the flow in a ventilated room, for example, where the velocities are very small, it is important to account correctly for buoyancy effects. The heat transfer at walls is, in some cases [2], essential for the performance of the ventilation system. Near heating or cooling walls the flow can be strongly affected by buoyancy, and the viscous effects are usually large. This means that conventional wall functions, which are based on the use of local equilibrium logarithmic velocity and temperature assumptions, are not applicable.

In the present study the flow in a tall two-dimensional cavity of 5:1 aspect ratio is calculated using finite volume methods. The results obtained are compared with experimental data from Cheesewright et al. [3, 4]. The CELS solver, which was developed and applied to buoyancy-driven flows by Galpin and Raithby [5], is used. The solver was originally formulated for flows where the Boussinesq approximation (small density variations) for the gravitational term is valid; as this is not the case in the present study, the solver is extended to handle large density variations.

The development of low Reynolds number turbulence models has, so far, been aimed at predicting low Reynolds number flows near walls. It is also important to be able to predict low Reynolds number flow in free recirculating flows. In ventilated rooms, for example, the velocities are small, and it is possible that the flow is not fully turbulent or that it can relaminarize due to buoyancy effects.

Lars Davidson's present address is CERFACS, 42 Avenue G. Coriolis, F-31057 Toulouse, France.

I thank Professor Erik Olsson (who has been my supervisor) for his help and support. I am also grateful to Docent Lennart Löfdahl for valuable comments. The Swedish Council for Building Research sponsored this work.

Copyright © 1990 by Hemisphere Publishing Corporation

NOMENCLATURE

c_μ, $c_{1\epsilon}$, $c_{2\epsilon}$	constants in the turbulence model
f_1, f_2, f_μ	damping functions in the turbulence model
g	acceleration due to gravity
G_B	buoyancy source term in the turbulence models
H	height of cavity
k	turbulent kinetic energy
L	length of cavity
n	coordinate in the normal direction from the wall
p	pressure
P_k	turbulence-generating source term in the k and ϵ equations
q	local heat transfer rate at the vertical walls per unit area, kW/m
Re_n	local Reynolds number ($= \rho\sqrt{k}n/\mu$)
Re_t	local Reynolds number [$= \rho k/(\mu\epsilon)$]
t	temperature, °C
u, v	mean velocity in x and y directions, respectively
u_*	friction velocity
u_i	mean velocity in x_i direction
x	horizontal Cartesian coordinate (see Fig. 1)
x^+	nondimensional distance from the wall, ($= xu_*/\nu$)
x_1	$= x$
x_2	$= y$
x_i	Cartesian coordinate in the i direction
y	vertical Cartesian coordinate (see Fig. 1)
α	contraction factor for the grid, Eq. (6)
β	coefficient of thermal expansion
ϵ	dissipation of turbulent kinetic energy
η	$= y$ at the hot wall; $= H - y$ at the cold wall
μ, μ_t, μ_{eff}	dynamic viscosity (laminar, turbulent, and effective, respectively)
ν	kinematic viscosity
ρ	density
σ_l	laminar Prandtl number
σ_k, σ_t, σ_ϵ	turbulent Prandtl number for k, t, and ϵ, respectively
τ	time
$\Delta\tau$	time step
$\Delta\tau^*$	nondimensional time step, Eq. (7)
τ_{ref}	reference time step, Eq. (7)
Ψ	stream function ($u = \partial\Psi/\partial y$)

Subscripts

C	cold wall
H	hot wall
max	maximum
ref	reference value for the room
w	wall

Superscript

o	referring to value at old time step

As a first step toward a turbulence model able to predict this type of flow, a modified form of a low Reynolds number k–ϵ model is developed. No near-wall terms are added to the equations in this model, and the damping equations include no irrelevant distance from the walls. It is hoped that this model can be used to predict free low Reynolds number flows, where the viscous effects are not due to walls.

The objectives of the present study are (1) to develop a modified form of a low Reynolds number k–ϵ model, as described above, that is consistent in its near-wall behavior and allows simulation of the decay of grid turbulence; (2) to test this model and the model of Lam and Bremhorst [1] in a flow driven by natural convection; to compare the predictions with the experimental data to investigate how well the models predict this type of flow and how well the models predict low Reynolds number phenomena such as transition and relaminarization; and (3) to investigate how efficient the modified CELS solver is in turbulent flow.

In the following sections, the solution procedure is described, the turbulence models are presented, the performances of CELS and SIMPLEC are compared, results are discussed, and conclusions are drawn.

SOLUTION PROCEDURE

The continuity, the momentum, and the temperature equations can be written as

$$\frac{\partial \rho}{\partial \tau} + \frac{\partial}{\partial x}(\rho u) + \frac{\partial}{\partial y}(\rho v) = 0 \tag{1a}$$

$$\begin{aligned}\frac{\partial}{\partial \tau}(\rho u) + \frac{\partial}{\partial x}(\rho u^2) + \frac{\partial}{\partial y}(\rho uv) \\ = -\frac{\partial p}{\partial x} + \frac{\partial}{\partial x}\left(\mu_{\text{eff}}\frac{\partial u}{\partial x}\right) + \frac{\partial}{\partial y}\left(\mu_{\text{eff}}\frac{\partial u}{\partial y}\right) \\ + \frac{\partial}{\partial x}\left(\mu_{\text{eff}}\frac{\partial u}{\partial x}\right) + \frac{\partial}{\partial y}\left(\mu_{\text{eff}}\frac{\partial v}{\partial x}\right) - \frac{2}{3}\frac{\partial}{\partial x}(\rho k)\end{aligned} \tag{1b}$$

$$\begin{aligned}\frac{\partial}{\partial \tau}(\rho v) + \frac{\partial}{\partial x}(\rho uv) + \frac{\partial}{\partial y}(\rho v^2) \\ = -\frac{\partial p}{\partial y} + \frac{\partial}{\partial x}\left(\mu_{\text{eff}}\frac{\partial v}{\partial x}\right) + \frac{\partial}{\partial y}\left(\mu_{\text{eff}}\frac{\partial v}{\partial y}\right) \\ + \frac{\partial}{\partial x}\left(\mu_{\text{eff}}\frac{\partial u}{\partial y}\right) + \frac{\partial}{\partial y}\left(\mu_{\text{eff}}\frac{\partial v}{\partial y}\right) - \frac{2}{3}\frac{\partial}{\partial y}(\rho k) - (\rho - \rho_{\text{ref}})g\end{aligned} \tag{1c}$$

$$\frac{\partial}{\partial \tau}(\rho t) + \frac{\partial}{\partial x}(\rho ut) + \frac{\partial}{\partial y}(\rho vt) = \frac{\partial}{\partial x}\left[\left(\frac{\mu}{\sigma_l} + \frac{\mu_t}{\sigma_t}\right)\frac{\partial t}{\partial x}\right] + \frac{\partial}{\partial y}\left[\left(\frac{\mu}{\sigma_l} + \frac{\mu_t}{\sigma_t}\right)\frac{\partial t}{\partial y}\right] \tag{1d}$$

where x is the horizontal direction and y is vertically upward. The density is calculated from the gas law, and the viscosity is calculated from Sutherland's formula:

$$\mu = \frac{1.458 \times 10^{-6}(t + 273)^{1.5}}{t + 383.4} \tag{1e}$$

Although only the steady solutions of Eq. (1) are of interest in this study, the equations are given in transient form, and the time step $\Delta\tau$ is used as a free parameter by which the convergence rate may be optimized. These equations are solved using the CELS method, combined with Newton-Raphson linearization of the convective terms in the temperature equation [5]; this linearization results in a temperature-to-velocity coupling that is lost when standard linearization methods are used. A Newton-Raphson linearization (i.e., a Taylor expansion ignoring terms of order higher than 1) of the product ut gives

$$ut \approx u^o t^o + \frac{\partial}{\partial u}(ut^o)(u - u^o) + \frac{\partial}{\partial t}(u^o t)(t - t^o) = u^o t + ut^o - u^o t^o \tag{2}$$

The original CELS method assumes that the Boussinesq approximation is valid for the gravitational term, which is not valid in the present study, since there exist temperature differences of up to 45°C. The gravitational term in the v equation is rewritten so that

$$-g(\rho - \rho_{ref}) = \rho_{ref} g\beta(t - t_{ref}) - g(\rho - \rho_{ref}) - \rho_{ref} g\beta(t - t_{ref})$$

where the first term on the righthand side of the equation was used in the CELS formulation and the two remaining terms were included in the constant source term.

The CELS method is described in detail in the works by Raithby's group [5–7], and more details on the present implementation of CELS can be found in [8].

LOW REYNOLDS NUMBER k–ϵ MODELS

The object here, as mentioned in the introduction, is to develop a low Reynolds number k–ϵ turbulence model able to handle viscous effects near walls and, hopefully, in free flows. The model should also be consistent in its near-wall behavior and in allowing simulation of grid turbulence. The viscous effects in free flows are due to low velocities that make the production term very small and/or to relaminarization caused by buoyancy effects (stable stratification); both these effects may occur in ventilated rooms [2].

The k and ϵ equations can be written

$$\frac{\partial}{\partial \tau}(\rho k) + \frac{\partial}{\partial x_i}(\rho u_i k) = \frac{\partial}{\partial x_i}\left(\mu + \frac{\mu_t}{\sigma_k}\right)\frac{\partial k}{\partial x_i} + P_k + G_B - \rho\epsilon \tag{3}$$

$$\frac{\partial}{\partial \tau}(\rho\epsilon) + \frac{\partial}{\partial x_i}(\rho u_i \epsilon) = \frac{\partial}{\partial x_i}\left(\mu + \frac{\mu_t}{\sigma_\epsilon}\right)\frac{\partial \epsilon}{\partial x_i} + \frac{\epsilon}{k}[f_1 c_{1\epsilon} P_k + c_{1\epsilon} G_B - f_2 c_{2\epsilon}\rho\epsilon] \tag{4}$$

where

$$x_1 = x \qquad x_2 = y$$

$$P_k = \mu_t\left[\frac{\partial u_i}{\partial x_j} + \frac{\partial u_j}{\partial x_i}\right]\frac{\partial u_i}{\partial x_j} \qquad G_B = -\frac{\mu_t g\beta}{\sigma_t}\frac{\partial t}{\partial y} \qquad \mu_t = \frac{f_\mu c_\mu \rho k^2}{\epsilon}$$

$$\sigma_k = 1.0 \qquad \sigma_\epsilon = 1.3 \qquad \sigma_t = 0.9 \qquad c_\mu = 0.09 \qquad c_{1\epsilon} = 1.44 \qquad c_{2\epsilon} = 1.92$$

Patel et al. [9] have tested a number of low Reynolds number k–ϵ models. They concluded that the model of Jones and Launder [10] (hereafter denoted JL) was the best and that the model of Lam and Bremhorst [1] (hereafter denoted LB) also gave results in good agreement with experiments. In the test case chosen in the present study, there are, according to experiments, transition regions from laminar to turbulent flow (as well as relaminarization). Rodi and Scheuerer [11] used the LB model for predicting the flow along turbine blades, and in that flow there was also a transition region, which the LB model was shown to predict well in agreement with experimental data. For these reasons the LB model has been chosen for the present study. The functions and the boundary conditions for the LB model are given below.

LB Model

$$f_\mu = [1 - \exp(-0.0165\mathrm{Re}_n)]^2 \left(1 + \frac{20.5}{\mathrm{Re}_t}\right) \qquad f_1 = 1 + \left(\frac{0.05}{f_\mu}\right)^3$$

$$f_2 = 1 - \exp(-\mathrm{Re}_t^2) \qquad \mathrm{Re}_t = \frac{\rho k^2}{\mu\epsilon} \qquad \mathrm{Re}_n = \frac{\rho\sqrt{k}n}{\mu}$$

where n is the normal distance from the nearest wall and $k = \partial\epsilon/\partial n = 0$ at walls.

In the original LB model, another boundary condition at the walls was used for the ϵ equation, namely,

$$\epsilon = \nu\frac{\partial^2 k}{\partial n^2} \tag{5}$$

The boundary condition used in the present work ($\partial\epsilon/\partial n = 0$, which is more convenient) was tested by Patel et al. [9], who found that this boundary condition gave the same results as Eq. (5).

Present Model

In the present model, as well as in the LB model, the physical (isotropic) dissipation is solved, and the same form of the f_1 function as in the LB model is chosen. The disadvantage of the LB model is that the f_μ function includes the distance from the wall. Since the f_μ function, according to Patel et al. [9], is the most important damping function, f_μ is taken from the JL model, i.e.,

$$f_\mu = \exp\left[-\frac{3.4}{(1 + \mathrm{Re}_t/50)^2}\right]$$

The object of the f_1 function is to increase the production of ϵ near the wall in order to decrease the turbulent kinetic energy. Since the f_μ function in the LB model damps the viscosity (and k) much more than f_μ in the JL model, the constant in the f_1 function ($=0.05$) has to be increased to increase ϵ so that the turbulent kinetic energy decreases. Values between 0.05 and 0.16 on the constant were tested, and the value 0.14 was found to be optimum.

There are three main requirements for the function f_2:

1. It should force the dissipation term in the ϵ equation to vanish at the wall.
2. In order to render the ϵ equation consistent at the wall, $f_2 \sim n^2$ is necessary [9].
3. The constant $c_{2\epsilon}$ is determined from the decay of isotropic grid turbulence, where $k \sim x^{-m}$, and $m = 1.25$ for high Reynolds numbers; in the final stage the exponent changes to $n = 2.5$, and the f_2 function must take this into account.

It may be noted that the f_2 function in the LB model meets only one of these requirements (it does go to zero at the wall). In the present model the form of the f_2 function is taken as

$$f_2 = [1 - 0.27 \exp(-\mathrm{Re}_t^2)][1 - \exp(-\mathrm{Re}_n)]$$

which meets all three requirements. The first term in square brackets changes, for low Reynolds numbers, the exponent in $k \sim x^{-m}$ from $m = 1.25$ to $m = 2.5$; regions where this occurs are normally far from walls, so that the second term should be close to 1 even if k is small. To show that, close to the wall, the second term of f_2 in square brackets $\sim n^2$, it is expanded in a Taylor series, so that

$$1 - \exp(-\mathrm{Re}_n) = \mathrm{Re}_n - \mathrm{Re}_n^2 + \cdots$$

The local Reynolds number is defined as $\mathrm{Re}_n = \sqrt{k}n/\nu$, and since $k \sim n^2$ close to the wall, it can be seen that $f_2 \sim n^2$ as required.

To summarize the present model, the functions and the boundary conditions are given:

$$f_\mu = \exp\left[-\frac{3.4}{(1 + \mathrm{Re}_t/50)^2}\right] \qquad f_1 = 1 + \left(\frac{0.14}{f_\mu}\right)^3$$

$$f_2 = [1 - 0.27 \exp(-\mathrm{Re}_t^2)][1 - \exp(-\mathrm{Re}_n)]$$

and $k = \partial\epsilon/\partial n = 0$ at walls.

COMPARISON OF CELS AND SIMPLEC

In this section the buoyancy-driven flow in a rectangular cavity (see Fig. 1) is calculated using CELS and SIMPLEC [12]. A transient formulation is adopted as a convenient means of introducing relaxation into the iterative solution. When, as in this study, only the steady-state solution is of interest, the time step $\Delta\tau$ is used as a free parameter by which the convergence rate may be optimized. An underrelaxing factor of 0.5 was, furthermore, used in the k and ϵ equations, as well as in updating the viscosity.

At each (false) time step the k and ϵ equations were solved after the u, v, t, and p equations (using CELS or SIMPLEC) had been solved. First the k equation was solved, then the ϵ equation, and finally, the viscosity was updated. This sequence (solving k and ϵ and updating μ) was carried out three times for each time step, which was found to increase the convergence rate both for CELS and SIMPLEC; perhaps three times is not optimal, but it was found to be superior to one time.

The grids were generated using Eq. (6), where the coordinates of the x grid lines, x_m, were set as

$$x_m = x_{\max}\left\{-0.5 \tanh\left[\alpha\left(2\frac{m}{n} - 1\right)\right]/\tanh(-\alpha) + 0.5\right\} \tag{6}$$

where n is the number of x lines and α is a contraction factor; the same formula was used for the y lines. A grid with 28 × 28 interior nodes (with $\alpha = 2$) and a 56 × 56-node grid ($\alpha = 3.5$) were used in this section. When using the coarse grid the standard high Reynolds number k–ϵ model [$f_\mu = f_1 = f_2 = 1$ in Eqs. (3)–(4)] was used to reduce the influence of the turbulence model on the convergence rate, and the boundary conditions at the walls were then prescribed using wall functions [13].

In Tables 1 and 2 the convergence data for CELS and SIMPLEC are summarized (all calculations were performed on a work station VAX-2000, which is approximately half as fast as VAX-785); for more details, see [8]. The time steps given in the tables are nondimensional, i.e. [5, 14],

$$\Delta\tau^* = \frac{\Delta\tau}{\tau_{\text{ref}}} \qquad \tau_{\text{ref}} = \left(g\beta\frac{\partial t}{\partial y}\right)^{-1/2} \tag{7}$$

where τ_{ref} was taken as the largest in the field. The size of τ_{ref} was approximately 0.2 and 0.35 s for the fine and coarse grids, respectively.

Two different schemes were tested: QUICK developed by Leonard [15] (the form of the coefficients for a nonuniform grid is given in [8]) and the hybrid/central differencing scheme (HDS) were both used in the u, v, and t equations. In the k and ϵ equations, only the HDS was used. The reason that QUICK was not used in the k and ϵ equations is twofold. First, the k and ϵ equations are rather insensitive to the choice of differencing scheme, since they are very source dominated [16], and second, QUICK can produce unphysical overshoots and undershoots, which could give negative values of k and ϵ, which, of course, is unphysical, and furthermore, normally leads rapidly to divergence in the iterative solution. From the tables, it can be seen that the CELS solver is much more efficient than SIMPLEC, especially in connection with the less stable QUICK scheme. Much larger time steps could be used with CELS than with SIMPLEC; the time steps presented in Tables 1 and 2 are the largest time steps with which convergence could be obtained (except when using CELS with HDS on the coarse grid, where infinitely large time steps

Table 1 Convergence Data for CELS and SIMPLEC
High Reynolds Number k–ϵ Model Together with Wall Functions

	CPU, hours	$\Delta\tau^*$	Number of time steps
	HDS on 28 × 28 Grid		
CELS	0.68	33	104
SIMPLEC	2.3	1.7	536
	HDS on 56 × 56 Grid		
CELS	21	6	713
SIMPLEC	~~23~~ 32	0.5	1875
	QUICK on 28 × 28 Grid		
CELS	2.35	1.7	339
SIMPLEC	9.5	0.3	1984

Table 2 Convergence Data for CELS and SIMPLEC. Present Low Reynolds Number k–ϵ Model

	CPU, hours	$\Delta\tau^*$	Number of time steps
	HDS on 56 × 56 Grid		
CELS	7.2	6	260
SIMPLEC	22.5	0.3	1221
	QUICK on 56 × 56 Grid		
CELS	7.8	3	264
SIMPLEC	40	0.003–0.15†	

Calculations were carried out using results obtained with the high Reynolds number k–ϵ model as initial fields.

†Various time steps were tested, but no convergent solution was obtained. The normalized residuals (see text) varied during the iteration procedure between 0.4 and 1.1.

could be used [8]). From Tables 1 and 2, it can be seen that for CELS the time steps should be on the order of, or slightly larger than, τ_{ref}, irrespective of turbulence model and differencing scheme. On the fine grid it was not possible to obtain a converged solution with SIMPLEC using QUICK together with the low Reynolds number k–ϵ model (see Table 2); no convergence problems were encountered with CELS.

A fixed number of sweeps performed by the CELS solver at each (false) time step was used, namely, five. The linear relaxation factor was set to 5 (see [5–8] for details).

RESULTS USING CELS AND LOW REYNOLDS NUMBER k–ϵ MODELS

In this section the buoyancy-driven flow in the cavity in Fig. 1 is calculated using the two different low Reynolds number k–ϵ models presented above. The CELS solver is

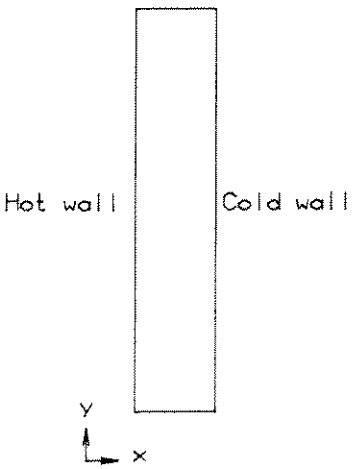

Fig. 1 Configuration using $t_H = 80°C$, $t_C = 34.2°C$, $H = 2.5$ m, $L = 0.5$ m. Vertical walls are isothermal, and horizontal walls are adiabatic.

used as described above, the QUICK scheme was used in the u, v, and t equations, and HDS was used in the k and ϵ equations. The results are presented in more detail in [8].

The calculated results are compared with the experiments by Cheesewright et al. [3], who made laser Doppler measurements in an air cavity with Rayleigh number 4×10^{10} [4] (this case has also been numerically simulated by Ince and Launder [17]). These experiments suffer from two problems: there is considerable heat loss through the sidewalls, and there is a small heat loss through the (well-insulated) top wall. Near the top wall the flow is exposed to a positive vertical temperature gradient, which acts to reduce the turbulent kinetic energy [see Eqs. (3–4)]; this should cause relaminarization (which occurs near the bottom wall). Due to the small heat loss through the top wall, the temperature gradient is reduced, and the expected relaminarization does not occur. This results in asymmetry of the flow in the experiments, and for this reason the comparison between calculations and experiments is concentrated at the midplane, where end effects should not be so large.

The heat loss through the sidewalls reduces the core temperature, which further increases the asymmetry of the flow in the experiments, i.e., the "diagonal symmetry" is lost (the flow in the upper right part of the cavity should be similar—or identical if temperature effects on density and laminar viscosity are not taken into account—to that in the lower left part of the cavity).

Grid and Convergence Criteria

A grid with 56×56 interior nodes is generated using Eq. (6) with $\alpha = 3.5$. It is important that the grid is sufficiently fine in the boundary layers at the vertical walls, where large gradients prevail. The grid used gives two grid lines with constant x located inside $x^+ = 1$ (i.e., near the vertical walls), which was considered sufficient.

The (absolute) residuals for the u, v, and t equations (the CELS solver ensures that the continuity equation is satisfied exactly at each time step) were summed for all cells and scaled with an appropriate value. For t the scaling value was taken as the total heat transfer through the hot wall, and for u and v the scaling value was calculated as

$$\sum_{x=0}^{x=L} |\dot{m}_i v_i|$$

at $y/H = 0.5$, where $\dot{m}_i$ is the vertical mass flux through control volume i. When the scaled residuals for the u, v, and t equations were all smaller than 0.5%, the solution was considered to be converged. Tests were made with convergence criteria of 0.1%, which gave a change in the calculated local heat transfer at the wall (see Fig. 5) of less than 0.1%.

Mean Velocities and Temperatures

In Fig. 2 the velocity field is presented in the form of contours of the stream function Ψ. The flow consists of a large clockwise vortex, and from the contours of the stream functions, it can be seen that there are two small clockwise vortices near the midplane $y/H = 0.5$. The calculated v profiles are compared with experimental data in Fig. 3. It

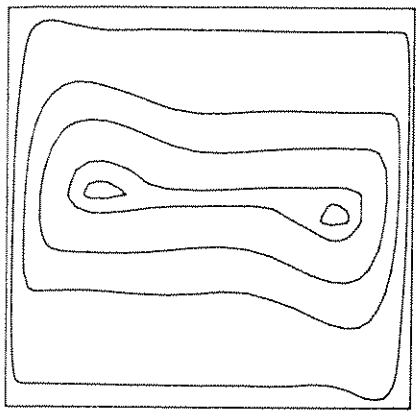

Fig. 2 Predicted contours of the stream function. Present model. Note change of scale in x direction (see Fig. 1).

can be seen that the agreement between prediction and experiments is good in the left half of the cavity and that predictions using the two different turbulence models are close to one another. The predictions with the LB model appear, in the core region, to be slightly better than those obtained with the present model, but both predicted profiles are probably within the bounds of experimental uncertainty. The sinusoidal form of the velocity profile near the midplane, predicted with the present model, is probably due to the fact that the predicted secondary vortices are stronger. The discrepancy between the predicted profiles and the experimental profile near the cold (right) wall is due to the aforementioned incomplete relaminarization at the top wall in the experiments. Careful examination of the predicted velocity profiles reveals a slight asymmetry in the predicted profiles as well. The velocity profiles near the hot wall are slightly fuller, which is to be expected, since (considering that the maximal velocities near the hot and the cold wall are the same; see Fig. 3) the density is greater near the cold wall than near the hot wall. It should be noted that the asymmetry in the predicted profiles is larger with the present model than with the LB model; this difference is discussed in the following section.

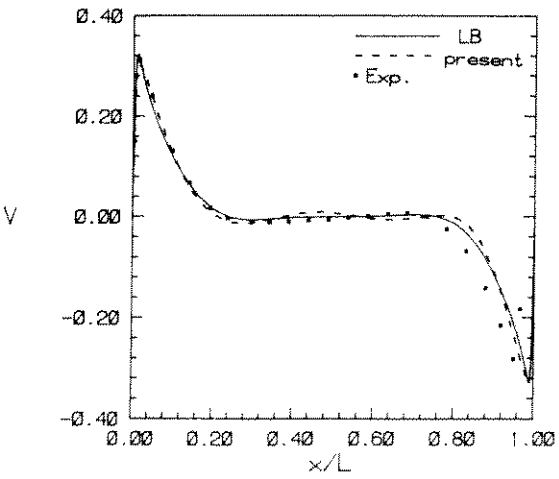

Fig. 3 Predicted and experimental v velocity profiles at $y/H = 0.5$. Experiments by Cheesewright et al. [3].

The predicted and experimental core temperatures are shown in Fig. 4, and it can be seen that the predicted core temperatures are nearly symmetric (as expected) in the sense that the local temperature difference $t_H - t_{core}$ at y is equal to $t_{core} - t_C$ at $H - y$. This symmetry is lost in the experiments due to heat loss through the side walls.

In Fig. 5 the predicted local heat transfer rates are compared with the experimental rate. First, it should be noted that the predicted local heat transfer rates along the hot and cold walls are close to equal. The predicted heat transfer rate along the hot wall is slightly larger than that at the cold wall because the laminar viscosity is higher at the hot wall [see Eq. (1*e*)]. The experimental local heat transfer rates along the two walls, however, differ considerably. This is due, as mentioned before, to heat loss through the sidewalls, which reduces the core temperature, and to the incomplete relaminarization near the top wall.

It can be seen in Fig. 5 that the predicted heat transfer rates at the vertical walls are larger with the present model than with the LB model because the predicted turbulent viscosity close to the wall is larger with the present model than with the LB model (see Fig. 7). The predicted heat transfer rate with the present model agrees rather well with experimental data at the hot wall (see Fig. 5*a*), but is higher at the cold wall. The predicted heat transfer rates with the LB model are lower than experimental data at the hot wall, and vice versa at the cold wall. It is to be expected that, due to heat losses through the sidewalls in the experiments, the experimental values should be too high at the hot wall and too low at the cold wall. Accordingly, the heat transfer rates predicted with the present model should be too high; however, due to problems in the experiments, no definite conclusion can be drawn as to whether the predicted local heat transfer rates with the present model are better or worse than those obtained with the LB model.

The present model predicts a sharp increase in q at $\eta/H \simeq 0.25$–0.3. The model predicts transition here. There is also a small "bump" in the curve for the LB model at $\eta/H \simeq 0.3$ at the hot wall, and this reflects a predicted transition region as well. This is in rather good agreement (slightly better for the present model) with the experiments [3], where a transition region was found at approximately $\eta/H \simeq 0.2$.

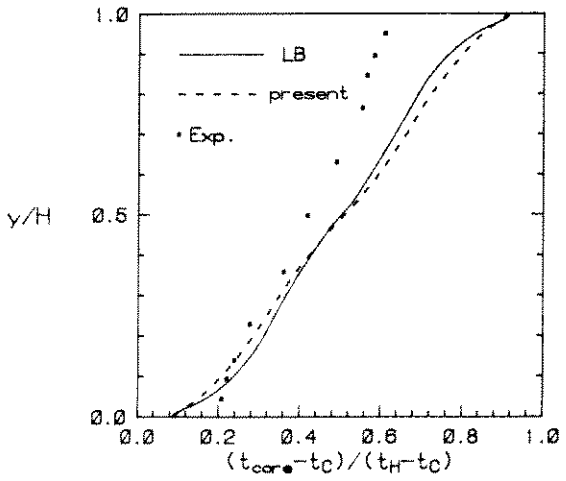

Fig. 4 Predicted and experimental local core temperatures. Experiments by Cheesewright et al. [3].

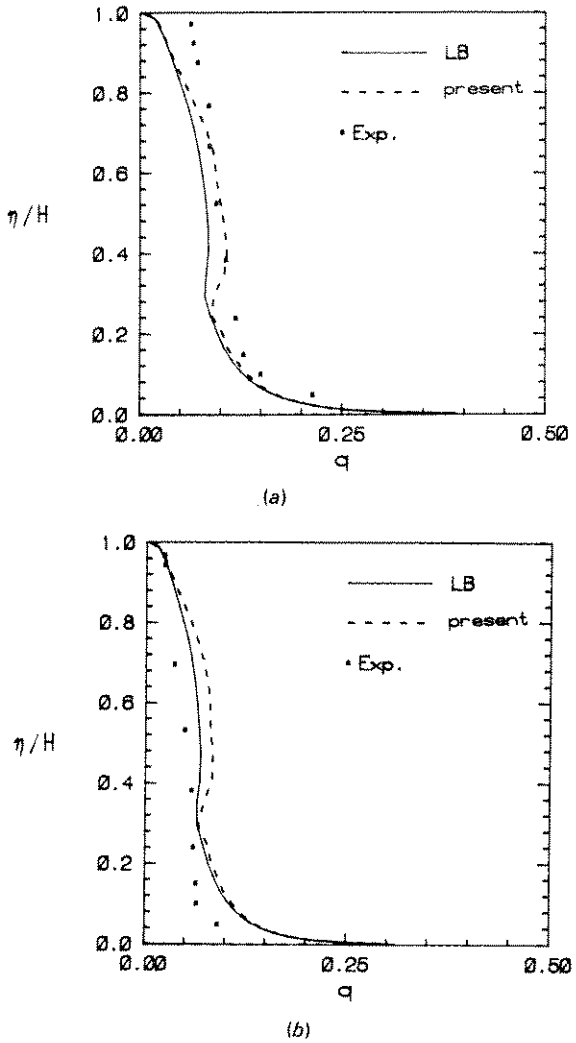

Fig. 5 Predicted and experimental local heat transfer rates at the vertical walls. Experiments by Cheesewright et al. [3]: (*a*) hot wall and (*b*) cold wall.

Turbulent Quantities

In Fig. 6 the predicted turbulent fluctuations are compared with experimental data, and both turbulence models perform well. Even though the experimental $\sqrt{k}$ profile is asymmetrical, it can probably be concluded that the turbulence models predict too high a turbulence level in the core region. Further, it can be seen that the predicted $\sqrt{k}$ profiles are, like the predicted v profiles (see Fig. 3), fuller near the hot wall than near the cold wall, and that the predicted $\sqrt{k}$ profile with the present model is more asymmetric than that predicted with the LB model; this is further discussed below.

Turbulent viscosity profiles at different vertical levels are presented in Fig. 7, which shows that the turbulent viscosity falls from a value of 15–20 μ at the top of the hot wall (bottom of the cold wall) to zero at the top of the cold wall (bottom of the hot wall).

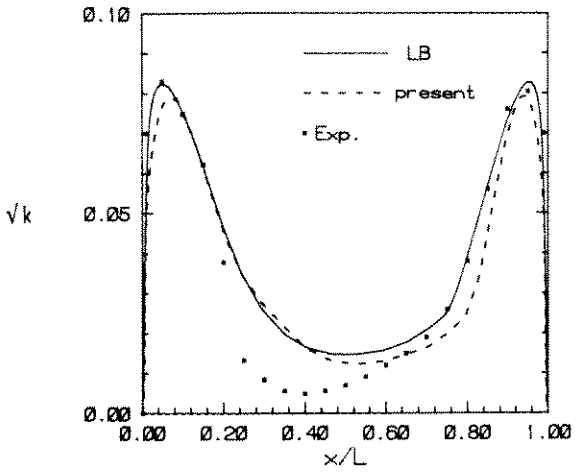

Fig. 6 Predicted and experimental turbulent fluctuations, $\sqrt{k}$, at $y/H = 0.5$. Experiments by Cheesewright et al. [3].

Close to the walls ($x/L \leq 0.04$ and $x/L \geq 0.96$), the turbulent viscosity predicted with the present model is higher than that predicted with the LB model, and vice versa farther from the walls. This is explained by the different f_μ functions; see Fig. 8. Close to the walls the f_μ function damps μ_t more in the LB model than in the present model, whereas the f_μ function in the present model is smaller farther from the walls.

In Fig. 5 the predicted heat transfer rate indicates a transition region near $\eta/H \simeq 0.25$–0.3. To further illustrate this, the predicted turbulent viscosity near the hot wall is shown in Fig. 9. Here it can be seen that at $y/H = 0.25$ the turbulent viscosity is just above zero, and that at $y/H = 0.3$ the turbulent viscosity has increased to approximately 5 μ.

In Figs. 10–11 the calculated turbulent kinetic energy budgets for the two turbulence models are shown. The dissipation term, $-\rho\epsilon$, attains a value (similar for the two models)

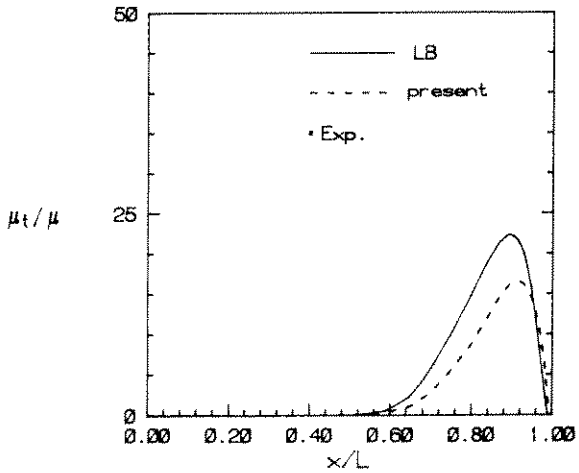

(a)

Fig. 7 Predicted turbulent viscosity scaled with the laminar viscosity: (*a*) $y/H = 0.1$.

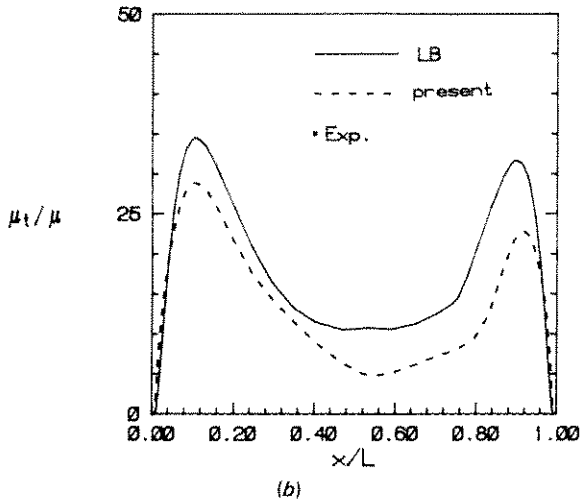

(b)

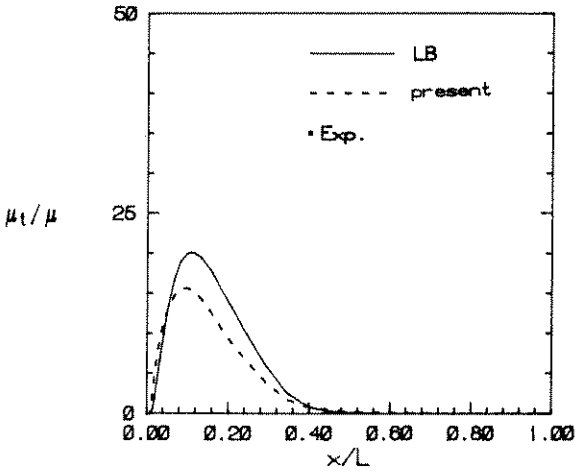

(c)

Fig. 7 Predicted turbulent viscosity scaled with the laminar viscosity (*Continued*): (*b*) $y/H = 0.5$, (*c*) $y/H = 0.9$.

at the wall according to the boundary condition $\partial\epsilon/\partial x = 0$. In a boundary layer the value of ϵ_w^+ at the wall, according to experiments, is $0.05 \leq \epsilon_w^+ \leq 0.1$, where

$$\epsilon_w^+ = \frac{\nu\epsilon_w}{u_*^4}$$

(see, e.g., [9]). The present model and the LB model give $\epsilon_w^+ = 0.016$ and $\epsilon_w^+ = 0.017$, respectively. The predicted values are thus considerably lower than the experimental values for a boundary layer, but it must be remembered that the two flows are rather different. The two models behave similarly for $0.04 \leq x/L \leq 0.96$, where the production term is balanced by the dissipation and diffusion terms. The present model gives larger ϵ near the cold wall than the LB model. This is due to the different constants in the f_1

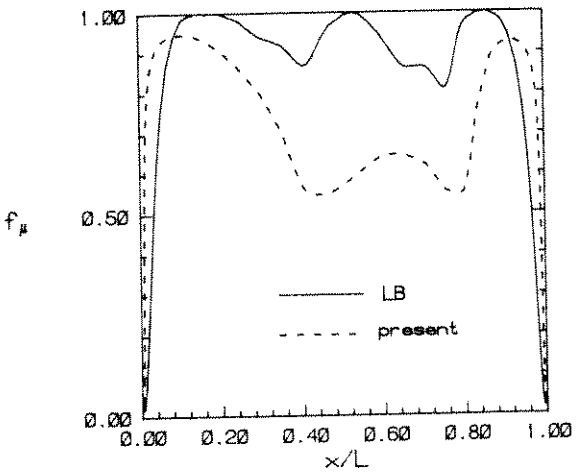

Fig. 8 The predicted f_μ functions; $y/H = 0.5$.

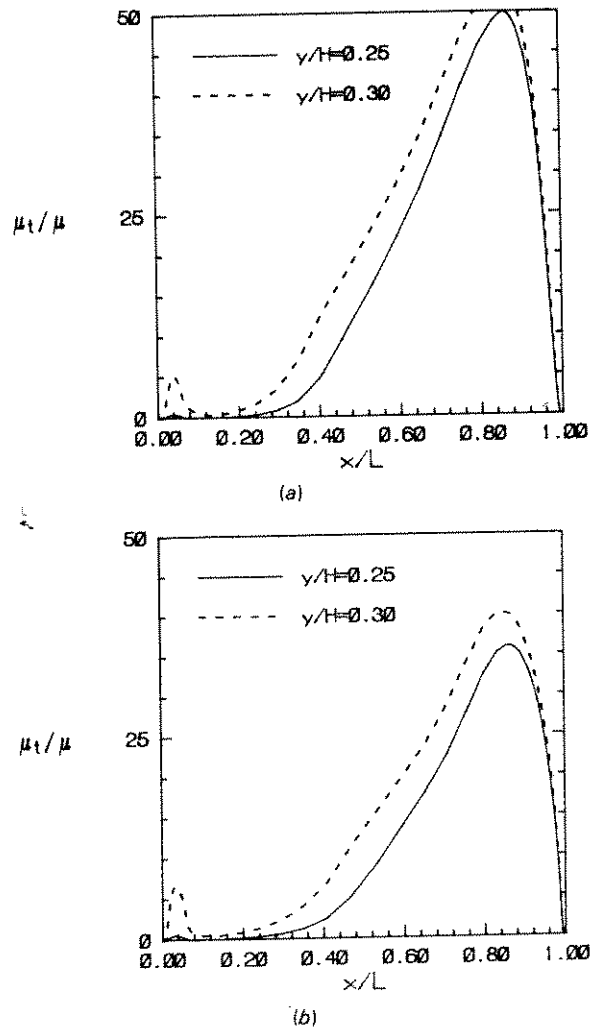

Fig. 9 Predicted turbulent viscosity near the hot wall: (*a*) LB model and (*b*) present model.

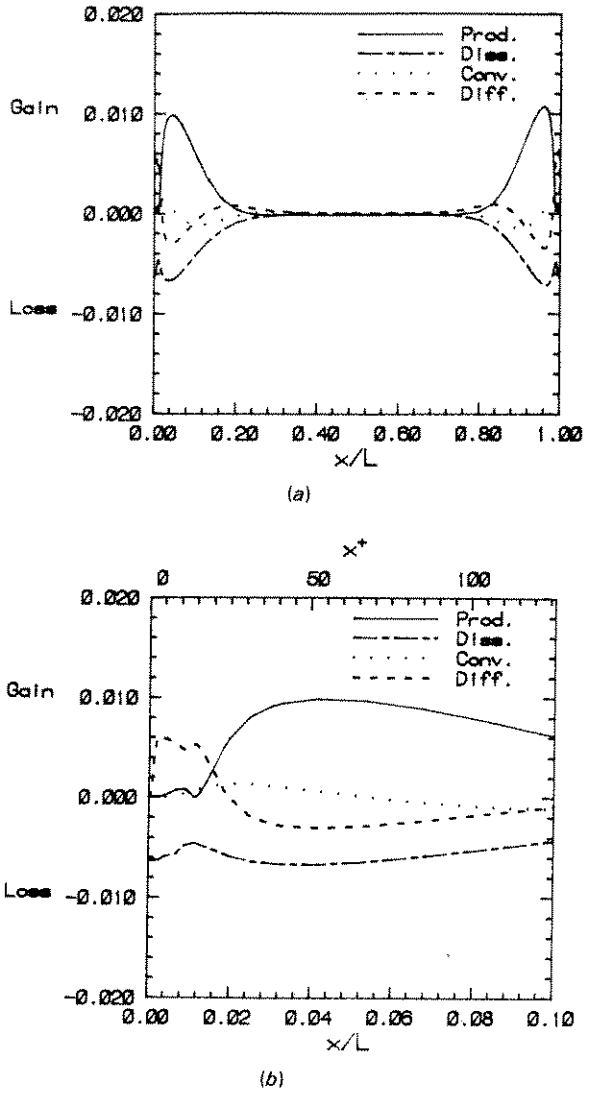

Fig. 10 Predicted turbulent kinetic budget at $y/H = 0.5$, $u_* = 0.0528$ for the LB model. Production is $P_k + G_B$, convection is $-\partial(\rho v k)/\partial y$, diffusion is $\partial/\partial x\,[(\mu + \mu_t/\sigma_k)\,\partial k/\partial x]$, and dissipation is $-\rho\epsilon$: (*a*) $0 \leq x/L \leq 1$ and (*b*) $0 \leq x/L \leq 0.1$.

function; f_1 is larger in the present model than in the LB model, and thereby the production of ϵ is larger. It can also be seen that the dissipation predicted with the present model is larger near the cold wall than near the hot wall. This is explained by the fact that the velocity profile (see Fig. 3) near the cold wall is sharper than near the hot wall, which gives larger production of ϵ near the cold wall. This is also true for the LB model, but here it is not so pronounced, since the constant in front of the production term in the ϵ equation is larger in the present model than in the LB model.

The high values on ϵ near the cold wall have been explained above by the sharp velocity gradients prevailing there; it can equally well be explained the other way around: high values on the dissipation give low turbulent viscosity, which in turn gives sharp velocity gradients. However, the important feature, when explaining the high values on

ϵ and the sharp velocity gradients, is the connection between them, and the f_1 function enhances this connection, especially in the present model.

In Figs. 10*b* and 11*b* the calculated turbulent kinetic energy budgets close to the hot wall for the two turbulence models are presented. In the LB model the dissipation and the diffusion balance each other for $x/L \leq 0.012$. In the present model, production increases close to the wall ($x/L = 0.01$) because the function f_μ does not damp k sufficiently; however, the f_1 function increases ϵ so that production at $x/L \simeq 0.008$ starts to fall off as the wall is approached. If the constant 0.05 is used in the f_1 function in the present model, the production term increases up to 0.05 at $x/L \simeq 0.004$.

It can be seen in Figs. 10*b* and 11*b* that the diffusion term close to the wall goes to zero instead of balancing the dissipation term. This problem is of a numerical nature and does not affect the predicted results, as the turbulence in this region is fully damped.

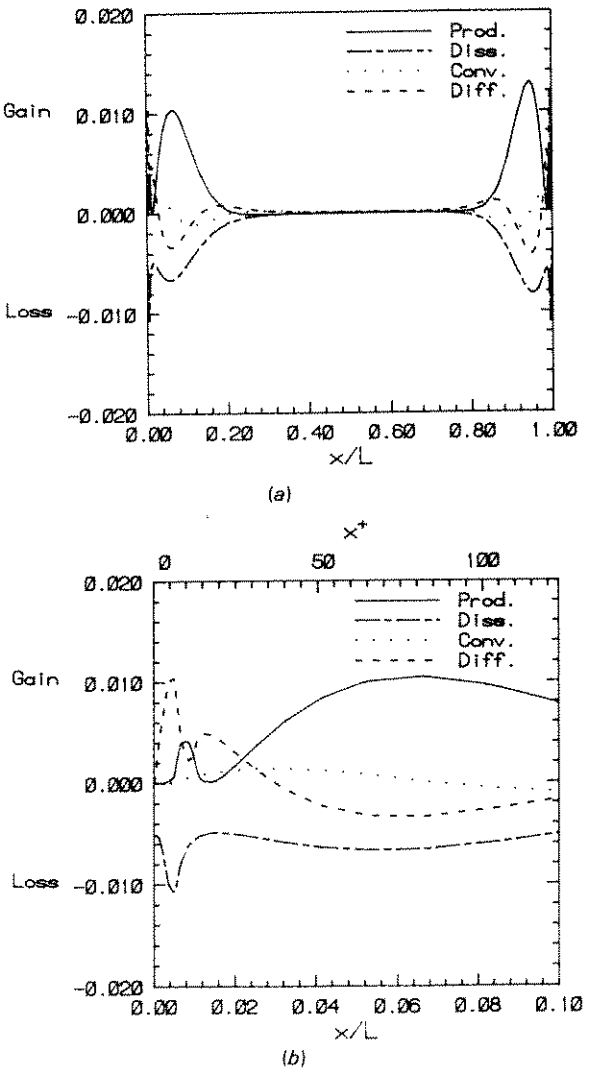

Fig. 11 Predicted turbulent kinetic budget at $y/H = 0.5$, $u_\tau = 0.0513$ for the LB model. Production is $P_k + G_B$, convection is $-\partial(\rho v k)/\partial y$, diffusion is $\partial/\partial x [(\mu + \mu_t/\sigma_k)\, \partial k/\partial x]$, and dissipation is $-\rho\epsilon$: (*a*) $0 \leq x/L \leq 1$ and (*b*) $0 \leq x/L \leq 0.1$.

The source term in the k equation is divided into one constant part (S_C) and one proportional part (S_P), so that the source can be written [18]

$$S = S_P k + S_C$$

where $S_P \leq 0$. All sinks (negative sources) must be included in S_P in order to prevent k from becoming negative. The dissipation term, $-\rho\epsilon$, is rewritten using the expression for μ_t (see section on low Reynolds number models, above), so that

$$-\rho\epsilon = -\rho^2 c_\mu f_\mu k^2/\mu_t$$

which gives

$$S_P = -\rho^2 c_\mu f_\mu k/\mu_t$$

Close to the wall, all turbulence is efficiently damped, which makes any linearization of the dissipation term inappropriate. In order to prevent a division by zero (in the expression for S_P) when $\mu_t \to 0$, a tiny value is added to μ_t in the denominator; thus the linearized dissipation term in the k equation goes to zero at the wall. Note that the dissipation, $-\epsilon$, rather than the linearized dissipation term in the k equation is plotted in Figs. 10 and 11; the linearized dissipation term balances, of course, the diffusion term.

CONCLUSIONS

The turbulent flow in a rectangular cavity with 5:1 aspect ratio and Rayleigh number of 4×10^{10} has been calculated using two different solution methods (CELS and SIMPLEC) and two different low Reynolds number k–ϵ turbulence models.

The CELS solver was originally formulated for flows where the Boussinesq approximation (small density variations) for the gravitational term is valid. As this is not the case in the present study, the solver was extended to handle large density variations.

A modified form of a low Reynolds number k–ϵ turbulence model that may have the capacity of predicting low Reynolds number effects in free flows has been developed. An example where this is of importance is in ventilated rooms [2], where the flow, far from walls, can relaminarize due to buoyancy. This model is consistent in its near-wall behavior, and it allows simulation of the decay of grid turbulence. The model of Lam and Bremhorst [1], which also is used, meets neither of these requirements.

The following conclusions can be made.

1. The modified CELS solver proved to be up to more than four times as fast as the SIMPLEC solver, and in one case (using QUICK and a low Reynolds number k–ϵ model on the fine grid), no convergent solution was obtained with SIMPLEC.
2. Considerably larger time steps could be used in CELS than in SIMPLEC.
3. The present model as well as the model of Lam and Bremhorst are shown to give results in good agreement with experimental data.
4. Flow along the vertical walls is, according to experiments [3, 19], characterized by a laminar, transitional, and fully turbulent region; both turbulence models predict these regions in agreement with experiments. The location of the transition region is slightly better predicted with the present model.

REFERENCES

1. C. K. G. Lam and K. A. Bremhorst, A Modified Form of the k–ϵ Model for Predicting Wall Turbulence, *J. Fluid Eng.*, vol. 103, pp. 456–460, 1981.
2. L. Davidson, Ventilation by Displacement in a Three-Dimensional Room: A Numerical Study, *Bldg. Environ.*, vol. 24, pp. 363–372, 1989.
3. R. Cheesewright, K. J. King, and S. Ziai, Experimental Data for the Validation of Computer Codes for the Prediction of Two-Dimensional Buoyant Cavity Flows, in *Significant Questions in Buoyance Affected Enclosure or Cavity Flows*, vol. HTD-60, pp. 75–81, American Society of Mechanical Engineers, New York, 1986.
4. R. Cheesewright, Personal communication, Dept. of Mech. Eng., Queen Mary College, London, 1988.
5. P. F. Galpin and G. D. Raithby, Numerical Solution of Problems in Incompressible Fluid Flow: Treatment of the Temperature-Velocity Coupling, *Numer. Heat Transfer*, vol. 10, pp. 105–129, 1986.
6. P. F. Galpin and G. D. Raithby, Treatment of Non-linearities in the Numerical Solution of the Incompressible Navier-Stokes Equations, *Int. J. Numer. Meth. Fluids*, vol. 6, pp. 409–426, 1986.
7. P. F. Galpin, J. P. Van Doormaal, and G. D. Raithby, Solution of the Incompressible Mass and Momentum Equations by Application of a Coupled Equation Line Solver, *Int. J. Numer. Meth. Fluids*, vol. 9, pp. 241–246, 1986.
8. L. Davidson, Numerical Simulation of Turbulent Flow in Ventilated Rooms, Ph.D. thesis, Dept. of Appl. Thermodyn. and Fluid Mech., Chalmers Univ. of Technol., Göteborg, 1989.
9. V. C. Patel, W. Rodi, and G. Scheuerer, Turbulence Models for Near-Wall and Low Reynolds Number Flows: A Review, *AIAA J.*, vol. 23, no. 9, pp. 1308–1319, 1986.
10. W. P. Jones and B. E. Launder, The Prediction of Laminarization with a Two-Equation Model of Turbulence, *Int. J. Mass Heat Transfer*, vol. 15, pp. 301–314, 1972.
11. W. Rodi and G. Scheuerer, Calculation of Heat Transfer to Convection-Cooled Gas Turbine Blades, *J. Eng. Gas Turbine Power*, vol. 107, pp. 620–626, 1985.
12. J. P. Van Doormaal and G. D. Raithby, Enhancements of the SIMPLE Method for Predicting Incompressible Fluid Flows, *Numer. Heat Transfer*, vol. 7, pp. 147–163, 1984.
13. W. Rodi, *Turbulence Models and Their Application in Hydraulics*, International Association of Hydraulic Research, Delft, 1980.
14. I. P. Jones, The Convergence of a Simple Iterative Strategy for Strongly Stratified Flows, in *Proc. 4th Int. Conf. on Numerical Methods in Laminar and Turbulent Flow*, Vol. 1, pp. 733–740, Swansea, 1985.
15. B. P. Leonard, A Stable and Accurate Convective Modeling Based on Quadratic Upstream Interpolation, *Comput. Meth. Appl. Mech. Eng.*, vol. 19, pp. 59–98, 1979.
16. M. A. Leschziner and W. Rodi, Calculation of Annular and Twin Parallel Jets Using Various Discretization Schemes and Turbulence-Model Variations, *ASME J. Eng.*, vol. 103, pp. 352–360, 1981.
17. N. Z. Ince and B. E. Launder, Computation of Turbulent Natural Convection in Closed Rectangular Cavities, in *2nd UK National Conference on Heat Transfer*, vol. 2, pp. 1389–1400, Univ. of Strathclyde, Glasgow, 1988.
18. S. V. Patankar, *Numerical Heat Transfer and Fluid Flow*, McGraw-Hill, New York, 1980.
19. P. W. Giel and F. W. Schmidt, An Experimental Study of High Rayleigh Number Natural Convection in an Enclosure, *Proc. 8th Int. Heat Transfer Conf.*, vol. 4, pp. 1459–1464, 1986.

Received 26 June 1989
Accepted 22 December 1989

Requests for reprints should be sent to L. Davidson.